RESEARCH ARTICLE SUMMARY

BRAIN DEVELOPMENT

Amplification of human interneuron progenitors promotes brain tumors and neurological defects

Oliver L. Eichmüller, Nina S. Corsini*, Ábel Vértesy, Ilaria Morassut, Theresa Scholl, Victoria-Elisabeth Gruber, Angela M. Peer, Julia Chu, Maria Novatchkova, Johannes A. Hainfellner, Mercedes F. Paredes, Martha Feucht, Jürgen A. Knoblich*

INTRODUCTION: Development of the human brain is protracted and involves distinct processes that have contributed to its large size and complexity. However, these changes might have also increased the vulnerability of the human brain to genetic disorders. Tuberous sclerosis complex (TSC) is a neurodevelopmental disorder characterized by debilitating neuropsychiatric symptoms, including epilepsy, autism, and intellectual disabilities. It involves distinct morphological aberrations in the brain such as the formation of benign subependymal tumors and dysplastic cortical lesions, which are commonly referred to as cortical tubers. TSC arises from mutations in the mechanistic target of rapamycin (mTOR) inhibitors TSC1 and TSC2 and is thought to be caused by elevated mTOR signaling activity.

RATIONALE: TSC is thought to originate from heterozygous TSC1/2 germline mutations followed by loss-of-function mutations that disrupt the second allele and cause somatic loss of heterozygosity (LOH). This hypothesis is generally supported by mouse models, but analysis of patient tissues revealed LOH only in tumors and rarely in the dysplastic regions. In addition, the animal models failed to recapitulate the full spectrum of pathognomonic lesions. We hypothesized that aspects of specifically human brain development rather than LOH could initiate the disease.

RESULTS: We generated a human model for TSC by growing cerebral organoids from patients who carried mutations in TSC2. The organoid model recapitulates the emergence of both brain tumors and dysplastic cortical regions. Using single-cell RNA-sequencing (scRNA-seq) and extensive histological validation, we identified a specific interneuron progenitor population that gives rise to both tumor and cortical tuber lesions. Comparisons of expression signatures with fetal brain scRNA-seq data revealed the origin of this cell type in the caudal ganglionic eminence (CGE) during mid-gestation. We therefore refer to this cell type as caudal late interneuron progenitor (CLIP) cells.

Our analysis uncovered particularly low amounts of TSC1/2 complex proteins in CLIP cells, making them susceptible to TSC1/2 levels. CLIP cells overproliferate and initiate both tumor and cortical tuber formation even when just one copy of TSC2 is lost. The second TSC2 allele can be mutated during tumor progression, but this does not occur through a second somatic mutation. Instead, it is caused by copy-neutral LOH (cnLOH), the exchange of large genomic regions between homologous chromosomes. CLIP cells depend on epidermal growth factor receptor (EGFR) signaling, and EGFR inhibition can revert the TSC phenotype, suggesting an alternative inroad to therapeutic intervention.

The sequence of events leading to TSC was validated in postmortem patient tissues. The seemingly confusing histological appearance of TSC brain lesions can be explained by the initiation of cortical lesions by CLIP cells and their derivatives, whereas other cell types contribute only at later stages. Thus, our analysis can explain the different mutational status of brain tumors and cortical tubers in TSC patients in the context of a common cell of origin.

CONCLUSION: This work shows that the analysis of neurodevelopmental genetic disorders can lead to fundamental mechanistic insights into human brain development. CLIP cells are identified as the shared cell of origin for brain lesions in TSC. The contribution of different lineages over time then generates the complex neurological defects observed in TSC. Although cnLOH occurs during TSC tumor progression, it is dispensable for disease initiation, demonstrating that the disease relevance of mutations should always be evaluated in the context of a specific cell of origin.

Human brain expansion was accompanied by a diversification of progenitor cell types. This work showcases an example of such a human progenitor cell type responsible for a human neurodevelopmental disease and demonstrates the necessity of using human models to identify disease mechanisms that involve processes not conserved in all mammals. ■

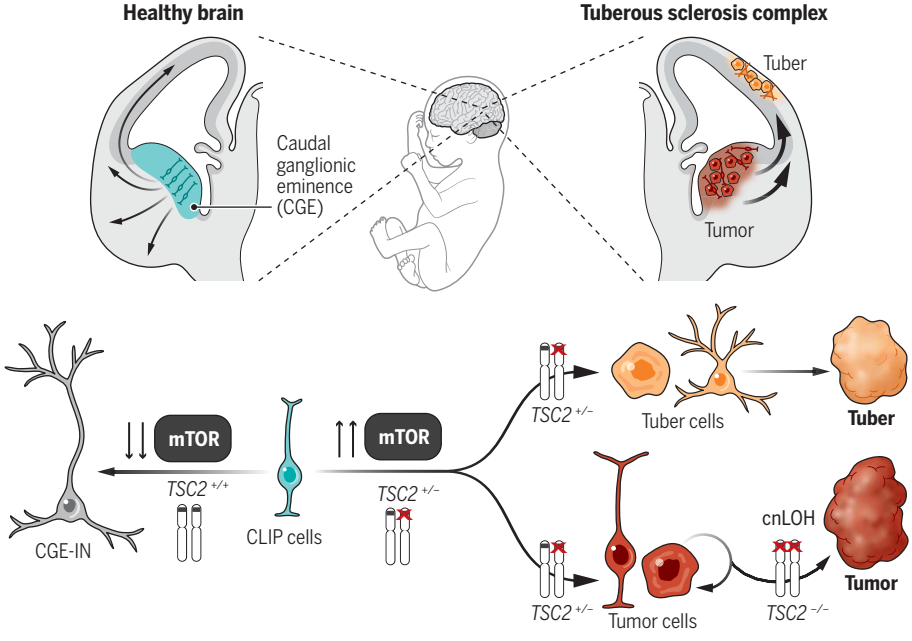

IMAGE: KELLIE HOLOSKI/*SCIENCE*

During mid-gestation, CLIP cells residing in the CGE generate interneurons that migrate into the cortex. (Top right) In TSC, CLIP cells generate brain tumors and cortical tubers. Heterozygous mutations in *TSC2* result in excessive proliferation of CLIP cells, generating cell types of cortical tubers (orange) as well as brain tumors (red). During progression, the healthy allele is lost because of cnLOH, increasing tumor proliferation.

The list of author affiliations is available in the full article online.
*Corresponding author. Email: nina.corsini@imba.oeaw.ac.at (N.S.C.); juergen.knoblich@imba.oeaw.ac.at (J.A.K.)
Cite this article as O. L. Eichmüller *et al.*, *Science* **375**, eabf5546 (2022). DOI: 10.1126/science.abf5546

READ THE FULL ARTICLE AT
https://doi.org/10.1126/science.abf5546

RESEARCH ARTICLE

BRAIN DEVELOPMENT

Amplification of human interneuron progenitors promotes brain tumors and neurological defects

Oliver L. Eichmüller[1,2], Nina S. Corsini[1]*, Ábel Vértesy[1], Ilaria Morassut[1], Theresa Scholl[3], Victoria-Elisabeth Gruber[3], Angela M. Peer[1], Julia Chu[4], Maria Novatchkova[1], Johannes A. Hainfellner[5], Mercedes F. Paredes[4], Martha Feucht[3], Jürgen A. Knoblich[1,5]*

Evolutionary development of the human brain is characterized by the expansion of various brain regions. Here, we show that developmental processes specific to humans are responsible for malformations of cortical development (MCDs), which result in developmental delay and epilepsy in children. We generated a human cerebral organoid model for tuberous sclerosis complex (TSC) and identified a specific neural stem cell type, caudal late interneuron progenitor (CLIP) cells. In TSC, CLIP cells overproliferate, generating excessive interneurons, brain tumors, and cortical malformations. Epidermal growth factor receptor inhibition reduces tumor burden, identifying potential treatment options for TSC and related disorders. The identification of CLIP cells reveals the extended interneuron generation in the human brain as a vulnerability for disease. In addition, this work demonstrates that analyzing MCDs can reveal fundamental insights into human-specific aspects of brain development.

Malformations of cortical development (MCDs) comprise varied neurodevelopmental disorders that cause more than 40% of medically refractory childhood seizures (*1*). Several MCDs—including hemimegalencephaly, focal cortical dysplasia IIb, and tuberous sclerosis complex (TSC)—are caused by mutations in mechanistic target of rapamycin (mTOR) pathway members, but their disease mechanisms remain elusive. TSC is a rare autosomal dominant disorder caused by mutation of either *TSC1* (hamartin) or *TSC2* (tuberin), which form a complex and inhibit the mTOR kinase. Patients suffer from debilitating, often drug-resistant neuropsychiatric symptoms, including intractable epileptic seizures, autism spectrum disorder (ASD), and intellectual disability (ID) (*2*). Most patients have focal dysplastic regions (cortical tubers) in the cortex, which consist of dysmorphic neurons, giant cells (GCs), and dysmorphic astrocytes (*3*, *4*). In addition, 80% of patients display subependymal nodules (SEN), benign tumors that form along the proliferative niches at the lateral ventricle and can develop into subependymal giant cell astrocytomas (SEGAs) (*5*). Analysis of human primary tissues suggested a common cell-of-origin for cortical tubers and SEN/SEGAs on the basis of shared transcriptomic alterations (*6*); however, the nature of this cell remains unclear. In mice, TSC pathogenesis is initiated through inactivation of the second allele of either *TSC1* or *TSC2* (*7*–*12*), and similar results have been obtained in spheroids (*13*). Genetic analysis in patients, however, revealed loss of the second allele in most SEN/SEGAs, but only few cortical tubers (*6*, *14*–*16*), challenging the previously suggested two-hit model (*7*, *17*). We hypothesized that these inconsistencies arise because cell types and processes specific to the human brain are critical for disease initiation. To identify those human-specific features, we generated human cerebral organoids (*18*) from patient-derived induced pluripotent stem cells (iPSCs) and compared our results with human primary material.

Cerebral organoids recapitulate TSC

To model the brain pathology of TSC, we derived iPSCs from patients with known *TSC2* mutations who suffer from drug-resistant epilepsy and show cortical tubers and subependymal tumors (Fig. 1A and fig. S1, A to C). Isogenic $TSC2^{+/+}$ lines were acquired directly from the germline mosaic first patient and generated by means of scarless CRISPR-based genome editing for the second patient (fig. S1, D, E, and H). Both patient mutations resulted in an early stop codon in regions commonly mutated in TSC (fig. S1, F and G). To study subependymal tumors, we cultured organoids in a high-nutrient (H) medium that promotes proliferation (Fig. 1B and indicated in all figures with an "H" by the staining panels). To examine the formation of cortical tubers, which emerge in less proliferative cortical regions, we transferred organoids to a low-nutrient (L) medium adapted from a published formulation (*19*) to three-dimensional culture (Fig. 1B and indicated in all figures with an "L" by the staining panels, and materials and methods).

We found no obvious differences between genotypes within the first 90 days of culture (fig. S2) corresponding to early phases of neurodevelopment, which is consistent with previous results (*13*); 110 days after embryoid body (EB) formation, however, nodular aggregates of cells expressing the proliferative marker Ki67 and the mTOR activation marker phospho-S6 (pS6) formed in $TSC2^{+/-}$ organoids cultured in H-medium (*$TSC2^{+/-}$ H-organoids)* (Fig. 1, D, G, and H; and fig. S3, A to F). These structures morphologically resembled SENs (Fig. 1C) (*20*–*22*). We validated the emergence of SEN-like tumors in organoids derived from a third TSC patient (Fig. 1, G and H, and fig. S3, C and D). SEN/SEGAs have been proposed to originate from an uncharacterized population of neural stem cells (NSCs) (*23*, *24*). To test for an NSC origin of SEN-like tumors in organoids, we stained for NSC markers. Expression of Nestin, ASCL1, and SOX2 (fig. S3, B, G, and H) demonstrated the NSC identity of SEN-like tumors in organoids.

To determine whether we could recapitulate the pathological cell types found in cortical tubers, we analyzed organoids cultured for 120 to 150 days in L-medium. In organoids derived from $TSC2^{+/-}$ cells, we found neurons with an enlarged soma and thickened processes similar to those of dysmorphic neurons in cortical tubers (Fig. 1, E and I, and fig. S4, A to D). After prolonged maturation in L-medium (~230 days), clusters of enlarged pS6-positive cells appeared (Fig. 1, F and J, and fig. S4, E to I). The morphology and expression of markers such as glial fibrillary acidic protein (GFAP) and Vimentin were reminiscent of GCs (*3*, *5*), which had characteristically low proliferation rates (Fig. 1F).

Dysmorphic astrocytes, a cell type previously identified in patient tubers, share marker expression with GCs but are morphologically distinct (*4*). In organoids, we identified individual enlarged GFAP-expressing cells morphologically similar to dysmorphic astrocytes with characteristic thickened and prolonged processes (fig. S4J). GCs expressed the neural progenitor marker Nestin (fig. S4F) (*24*), and almost all enlarged GFAP cells (GCs and dysmorphic astrocytes) in organoids expressed SOX2, suggesting a neural progenitor identity (patient 1, 99.7%; patient 2, 96%) (fig. S4, J and K).

Both cortical and tumor lesions were detected in H- and L-medium organoids (figs. S3I and S4L); however, the use of two different culturing conditions favored the emergence of the two specific phenotypes. Thus, organoids derived from $TSC2^{+/-}$ hiPSCs recapitulate the major histopathological features found in the brain of TSC patients.

[1]Institute of Molecular Biotechnology (IMBA), Austrian Academy of Sciences, Vienna Biocenter (VBC), Vienna, Austria. [2]University of Heidelberg, Heidelberg, Germany. [3]Department of Pediatric and Adolescent Medicine, Medical University of Vienna, Vienna, Austria. [4]Department of Neurology, University of California, San Francisco, San Francisco, CA, USA. [5]Department of Neurology, Medical University of Vienna, Vienna, Austria.
*Corresponding author. Email: nina.corsini@imba.oeaw.ac.at (N.S.C.); juergen.knoblich@imba.oeaw.ac.at (J.A.K.)

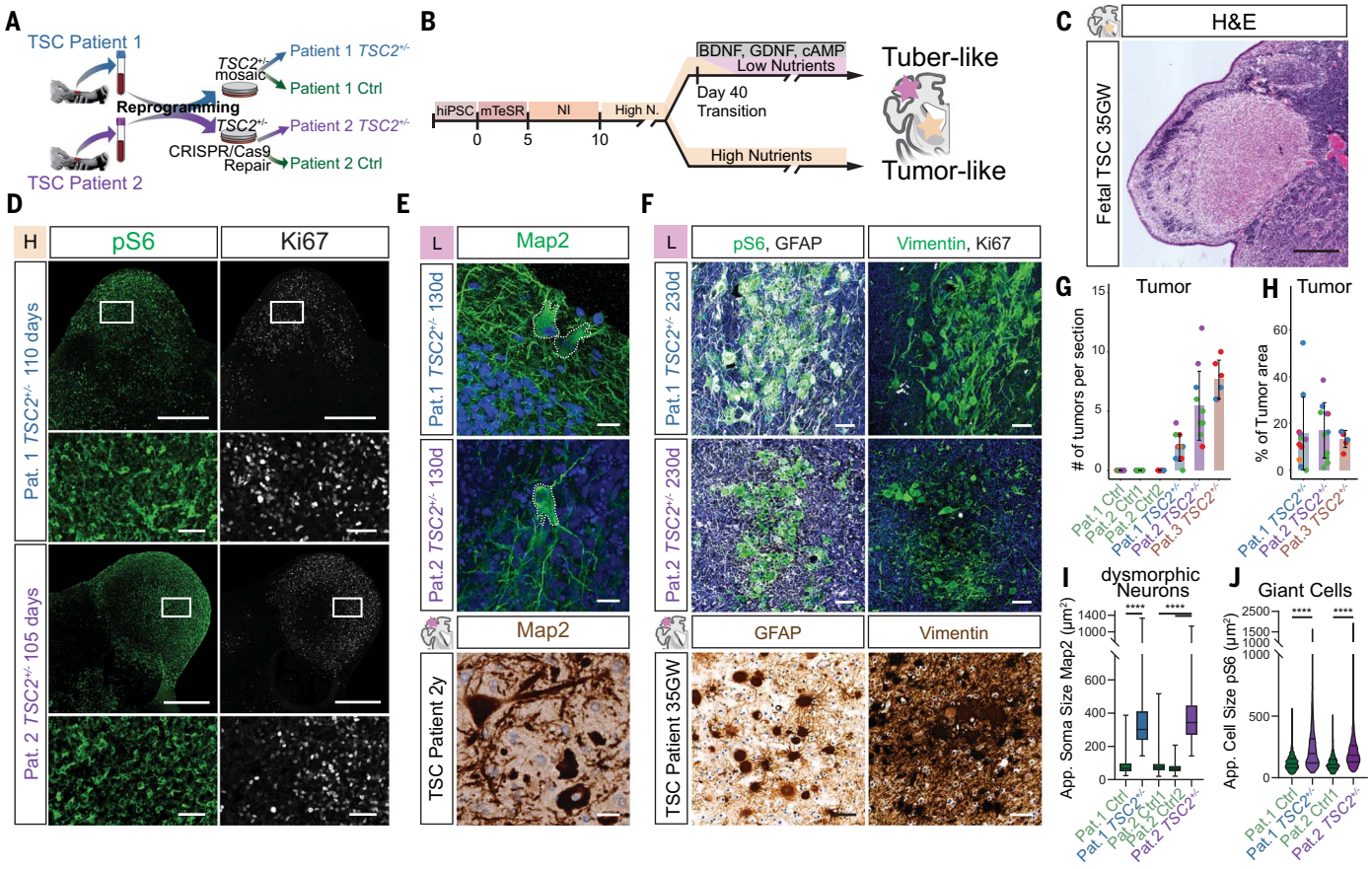

Fig. 1. *TSC2*$^{+/-}$-derived organoids recapitulate histopathology of TSC. (**A**) Control (Ctrl) and *TSC2*$^{+/-}$ cell lines derived from two patients (supplementary materials, materials and methods). (**B**) High- and low-nutrient organoid protocols used to model distinct TSC phenotypes. (**C**) Hematoxylin and eosin (H&E) staining of 35GW fetal brain depicts histopathology of a fetal SEN. (**D**) pS6 and Ki67 staining on 110- and 105-day-old *TSC2*$^{+/-}$-derived organoids in high-nutrient medium identifies SEN-like structures. (Bottom) Higher magnification of inset. (**E**) (Top) Map2 staining on 130-day-old organoids in L-medium shows dysmorphic neurons, with morphology comparable with those in (bottom) a resected tuber of a 2-year-old patient. Nuclear counterstain was performed with 4′,6-diamidino-2-phenylindole (DAPI) or hematoxylin. (**F**) pS6 and GFAP identifies GCs in 230-day-old organoids comparable with GCs in patient tubers. GCs in organoids express Vimentin, as shown in patients. GCs can be distinguished from tumors by their lower expression of Ki67. Nuclear counterstain was performed with DAPI or hematoxylin. (**G**) Tumors identified as pS6- and Ki67-positive areas are found in *TSC2*$^{+/-}$-derived organoids of all three patients. Control organoids of patient 1 and two clones of repaired patient 2 showed no tumors. Color of dots indicate independent batches of experiments (a summary of replicates is available in fig. S3E). (**H**) Percentage of tumor area of the total organoid area reveals similar tumor burden for organoids derived from three *TSC2*$^{+/-}$ patients. Color of dots indicate independent batches of experiments (a summary of replicates is available in fig. S3F). (**I**) Area of the soma in Map2^{+} neurons shows that dysmorphic neurons in *TSC2*$^{+/-}$-derived organoids are roughly fourfold larger then Map2^{+} neurons in control organoids [patient 1 control versus *TSC2*$^{+/-}$ $P < 0.0001$; patient 2 control 1 versus *TSC2*$^{+/-}$ and patient 2 control 2 versus *TSC2*$^{+/-}$ both $P < 0.0001$; ordinary one-way analysis of variance (ANOVA)] a summary of replicates is available in fig. S4D). (**J**) Cell area of pS6-positive cells shows enlarged pS6 cells in *TSC2*$^{+/-}$-derived organoids. (patient 1 control versus *TSC2*$^{+/-}$ $P < 0.0001$, patient 2 control versus *TSC2*$^{+/-}$ $P < 0.0001$, patient 1 control versus patient 2 control $P > 0.9999$, patient 1 *TSC2*$^{+/-}$ versus patient 2 *TSC2*$^{+/-}$ $P > 0.9999$; Kruskal-Wallis test with Dunn's multiple comparisons test) (a summary of replicates is available in fig. S4E) Scale bars, (C) and (D) 500 µm; (E) 20 µm; and (D), inset, and (F), inset, 50 µm.

Interneuron progenitors in TSC tumors

To characterize the cellular composition of tumors in TSC organoids, we performed single-cell transcriptomic analysis on 220-day-old organoids grown in H-medium. At this age, organoids consist almost exclusively of tumor tissues (fig. S5A). To compare intertumoral heterogeneity, three organoids were dissected into three tumor regions each and barcoded separately (*25*). Unsupervised clustering in UMAP projection identified four main clusters: interneurons (cluster 1), interneuron progenitors (cluster 2), dividing interneuron progenitors (cluster 3), and excitatory neurons (cluster 4) (Fig. 2A). Interneurons were characterized by the expression of canonical regulators of interneuron development such as *DLX2*, *DLX5*, and *DLX6-AS1* (Fig. 2C and fig. S5B). Interneuron progenitors expressed *DLX2*; *EGFR*; and progenitor markers such as *HES1*, *SLC1A3*, or *VIM* (Fig. 2C and fig. S5B). Dividing progenitors of the interneuron lineage were characterized by additionally expressing markers such as *MKI67* and *TOP2A* (Fig. 2C and fig. S5B). Only a very small number of excitatory lineage cells (cluster 4) were detected (3%) (Fig. 2B), marked by the expression of *NEUROD2* and *NEUROD6* (fig. S5B). Thus, tumors in *TSC2*$^{+/-}$ H-organoids consist mainly of progenitors and interneurons of ventral origin (Fig. 2C).

To investigate intertumoral heterogeneity, we compared the barcoded tumor regions. The cell type composition was highly consistent among the ventral lineage clusters, with all barcodes being evenly distributed (Fig. 2B and fig. S5, C and D). Whereas in the traditional view of tumorigenesis, in which TSC inactivation of the second allele is thought to be a

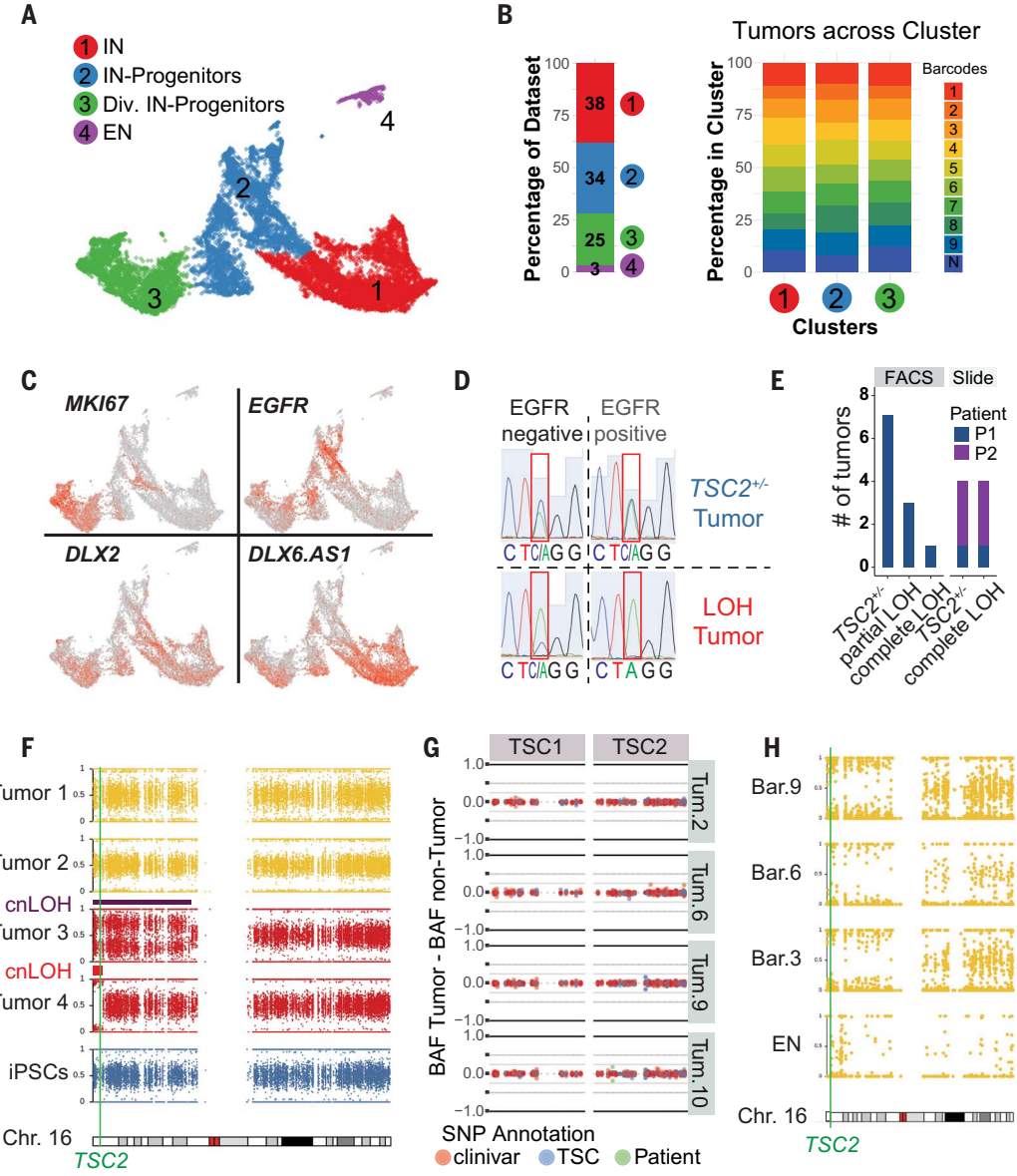

Fig. 2. TSC tumors consist of interneuron progenitors and acquire cnLOH during progression. (**A**) UMAP projection of cells isolated from 220-day-old TSC tumor organoids identified four main clusters: interneurons (cluster 1), interneuron progenitors (cluster 2), dividing interneuron progenitors (cluster 3), and excitatory neurons (cluster 4). (**B**) Dataset composition and contribution of different tumor regions. Of cells in tumors, 97% were ventral cells, and all nine tumor regions of three organoids were similarly distributed across ventral clusters (clusters 1, 2, and 3). (**C**) Expression of genes specific for dividing cells (*MKI67*) and interneurons (*DLX2* and *DLX6.AS1*) in 220-day-old TSC tumors. *EGFR* was specifically expressed in TSC tumor progenitors. (**D**) Genotyping example of FACS-sorted tumor ($EGFR^+$) and nontumor ($EGFR^-$) population, showing a heterozygous tumor and a LOH tumor that lost the wild-type (WT) allele (C) within the tumor. (**E**) Genotyping of tumors of patient 1 in FACS-sorted samples showing that 7 out of 11 TSC tumors were heterozygous, three showed a partial LOH, and one tumor showed a full LOH. Genotyping tumors from stained slides confirmed the presence of heterozygous and LOH tumors (patient 1, one $TSC2^{+/-}$ tumor and one LOH tumor; patient 2, three $TSC2^{+/-}$ tumors and three LOH tumors). (**F**) B-allele frequency (BAF) of chromosome 16 for four tumors of patient 1 $TSC2^{+/-}$-derived organoids. Whereas tumors 1 and 2 remain heterozygous, a shift in BAF is seen in tumors 3 and 4 compared with iPSCs. BAF and log R ratio (LRR) are provided in fig. S6L. Tumor 2 showed a partial cnLOH of a large section, whereas tumor 4 had a small complete cnLOH at the beginning of chromosome 16. Both cnLOH regions included the *TSC2* gene. (**G**) Targeted amplification of *TSC1* and *TSC2* in four tumors and matched nontumor samples of patient 1. Detected SNPs are colored as annotation of clinivar database (red), Leiden Open Variation Database (LOVD) TSC database (blue), or disease-causing SNP of patient 1 (green). The difference between BAF of the tumor and matched nontumor sample is shown. No disease-causing SNPs increased in the tumor samples could be detected. In tumor 10, there was a small shift of the patient SNP, which was confirmed as partial cnLOH (fig. S6I). (**H**) SNP mapping of scRNA-seq data shown in (A). Cells from tumors with sufficient reads (barcodes 3, 6, and 9) and excitatory neurons were aggregated per group, and allelic frequencies were determined. All tumors showed cnLOH, whereas excitatory neurons [(A), cluster 4] remained heterozygous.

prerequisite for causing the disease (7), our data suggest that a specific cell type that is sensitive to levels of mTOR signaling gives rise to TSC tumors.

Copy-neutral loss of heterozygosity in TSC tumors

To determine whether biallelic inactivation is required for the initiation of tumor lesions, we tested the mutational status of $TSC2^{+/-}$-derived organoids grown in H-medium at earlier stages (135 to 160 days). Tumor cells were isolated from patient 1 mutant organoids by means of fluorescence-activated cell sorting (FACS) for epidermal growth factor receptor (EGFR) (fig. S6, A to D and F to H), which was highly expressed on the interneuron progenitor cells in dissected tumors (Fig. 2C and fig. S6E). Genotyping of the *TSC2* locus indicated that many tumors remained heterozygous (Fig. 2, D and E, and fig. S6, I to K). In organoids from patient 1, we identified complete loss of heterozygosity (LOH) in one tumor and partial LOH in three tumors (Fig. 2E and fig. S6I). Additionally, we genotyped tumor sections and confirmed LOH in a subset of tumors of patients 1 and 2 (Fig. 2E and fig. S6, J and K).

To analyze recombination events in TSC tumors, we performed whole-genome sequencing (WGS) on two heterozygous and two LOH tumor samples (Fig. 2F and fig. S6, L and M).

WGS revealed no major genomic rearrangements in heterozygous tumors (Fig. 2F and fig. S6, L and M). By contrast, in LOH tumors extensive regions of chromosome 16, ranging from the telomere to and beyond the *TSC2* locus, had become homozygous through copy-neutral LOH (cnLOH) (Fig. 2F and fig. S6, L and M), the same genomic event resulting in LOH in TSC patients (*6*).

To test whether heterozygous tumors acquired second-hit mutations, we performed targeted amplification of *TSC1* and *TSC2* on four tumors and matched controls of patient 1 (Fig. 2G). No other pathogenic single-nucleotide polymorphisms (SNPs) were increased in tumor samples (Fig. 2G). Thus, a second hit at the *TSC1* or *TSC2* locus is not required for tumor initiation.

To probe whether cnLOH occurred at later stages during tumor progression, we investigated allelic frequencies in the 220-day-old single-cell RNA-sequencing (scRNA-seq) data (Fig. 2H). Tumor cells aggregated per barcode showed cnLOH in all tumors (Fig. 2H). Excitatory neurons (Fig. 2A, cluster 4) did not show cnLOH, further supporting an interneuron origin of TSC tumors (Fig. 2H). Thus, tumors in TSC organoids initiated from a heterozygous interneuron progenitor and acquired cnLOH only during progression.

To investigate whether cnLOH was required for the formation of cortical tuber-like structures, we analyzed GCs in 230-day-old $TSC2^{+/-}$ organoids. TSC2 protein expression was detected in more than 98% of GCs by using an antibody that recognizes only the wild-type TSC2 variant (patient 1, 98.4%; patient 2, 98.7%) (fig. S7, A to C). TSC2 protein was also expressed in GCs in fetal cortical tubers (fig. S7D), which is consistent with previous data (*26*, *27*). This suggests that second-hit events are not a prerequisite for tuber formation. Thus, although previous studies in mice have defined LOH in *Tsc1* (*8*, *9*, *11*, *12*, *28*) or *Tsc2* (*10*) as a requirement for TSC-like phenotypes, our data demonstrate that in human tissues, biallelic inactivation is dispensable for disease initiation. Our observations are consistent with reports that identify biallelic inactivation in subependymal tumors but rarely in cortical tubers (*6*, *14*–*16*, *29*, *30*).

Given that tumorigenesis in TSC organoids did not require cnLOH, we hypothesized that low amounts of TSC1/2 complex could sensitize interneuron progenitors to further reduction of TSC1 or TSC2. We observed reduced TSC2 in EGFR-positive interneuron progenitors in both control and in $TSC2^{+/-}$-derived organoids from both patients grown in H-medium (fig. S7, E to H) by using immunofluorescence. To quantitate TSC1 and TSC2 protein amounts, we performed targeted parallel reaction monitoring mass spectrometry (tPRM-MS) on FACS-sorted samples from patient 1 in H-medium. Both in control and $TSC2^{+/-}$-derived organoids, TSC1 and TSC2 were lower in EGFR-positive samples than in EGFR-negative samples (fig. S7J). Comparing EGFR-positive populations, we observed that whereas TSC1 was expressed at similar levels, TSC2 was significantly more down-regulated in EGFR-positive cells in the *TSC2* mutant as compared with the control population (fig. S7K). Thus, although in control organoids both components of the TSC complex were equally reduced, in TSC tumor cells, loss of one functional *TSC2* allele led to disproportional reduction of TSC2. These data suggest that interneuron progenitors have low levels of TSC proteins, which could sensitize them to heterozygous mutations in TSC genes.

The developmental trajectories of tumors and tubers

To determine whether tumors and tubers have a common cell of origin, we investigated H- and L-organoids at 110 days, when the TSC phenotypes were beginning to emerge (fig. S8, E to G). We integrated these data with the 220-day-old TSC tumor dataset (Fig. 3A). Unsupervised clustering in UMAP projection identified dorsal progenitor cells (clusters 3, 10, and 12), excitatory neurons (clusters 1, 2, 4, and 14), interneuron progenitor cells, and interneurons (clusters 5 to 9, 11, 13, 16, and 17), and cells resembling pre–oligodendrocyte-progenitor (OPC)–like cells (cluster 15) (Fig. 3A and fig. S8, B and C) (*31*). The 220-day-old TSC tumors contributed almost exclusively to the clusters that contained interneuron progenitor cells and interneurons (clusters 5 to 9, 11, and 13) (Fig. 3B). The same clusters were more abundant in 110-day-old $TSC2^{+/-}$ H- and L-organoids compared with control organoids: $TSC2^{+/-}$ H-organoids had more progenitor cells (clusters 5, 7, 11, and 13) (Fig. 3B), whereas in $TSC2^{+/-}$ L-organoids, mature interneurons were substantially increased (clusters 9 and 16) (Fig. 3B). Pre-OPC-like cells (Cl. 15) were slightly increased in 110-day-old TSC organoids. However, this cell type did not show morphological changes (fig. S9F). Thus, OPC lineages did not seem to contribute to TSC lesions in organoids.

To confirm that cnLOH was not required for the initiation of TSC phenotypes, we tested allelic frequencies in the d110 scRNA-seq datasets. Interneuron progenitors in $TSC2^{+/-}$ datasets did not show cnLOH, which is consistent with a disease initiation from a heterozygous progenitor (fig. S8H). This suggests that expansion of a common interneuron progenitor rather than cnLOH initiates tumor and tuber phenotypes.

To characterize the common cell of origin, we analyzed the gene expression signatures of the cells overrepresented in TSC organoids. Expression of markers such as *DLX2*, *DLX5*, *SP8*, *COUP-TFII* (*NR2F2*), and *SCGN* (fig. S8, B and D) revealed that this lineage originated from the caudal ganglionic eminence (CGE), a region in the ventral forebrain. The quiescent CGE progenitors (cluster 7) also expressed markers previously not found in interneuron progenitors, such as *EDNRB* and *PTGDS* (fig. S8D).

To investigate the developmental trajectories of these populations, we performed RNA velocity and pseudotime analysis (Fig. 3C and fig. S9, A to E). RNA velocity revealed a major trajectory toward CGE interneurons and a small bifurcation of CGE progenitors toward pre-OPC cells (Fig. 3C). Along the CGE lineage, we found expression of markers for quiescent (*GFAP*, *HOPX* together with *EDNRB* and *PTGDS*) and activated progenitors (*EGFR* and *DLX2*) and CGE interneurons (*DLX6-AS1* and *SCGN*) in both control and $TSC2^{+/-}$ organoids (Fig. 3D and fig. S9C). The small trajectory toward pre-OPC cells showed markers recently described for human pre-OPC lineages (fig. S9, D and E) (*31*).

Both tumor and tuber organoids shared the trajectory from CGE progenitors to CGE interneurons (Fig. 3C). To test whether lesion-specific cell types emerge, we investigated the trajectories within interneurons as determined from RNA velocity (Fig. 3C). We found that mature interneurons were separated into tumor- and tuber-enriched interneurons (fig. S10, A to F). Tumor interneurons were enriched in Gene Ontology (GO) terms related to ribosomal proteins and translation, whereas tuber interneurons showed specific up-regulation related to synapse formation and activity (fig. S10, G to O).

Although the descriptive nature of our scRNA-seq experiments limits their generalizability, these data indicate that interneuron progenitors that are increased in TSC follow defined developmental trajectories and diverge into lesion-specific interneuron subtypes.

Therefore, to determine whether the common developmental trajectory is present in the human fetal brain, we integrated our data with published scRNA-seq data from different fetal ages (fig. S11A) (*32*). Coclustering revealed similar cell types in the fetal brain (fig. S11, A and B), and pseudotime analysis confirmed trajectories toward interneurons and OPC cells (fig. S11, B and C). We found similar gene expression cascades along the neurogenic trajectory, with markers of quiescent progenitors expressed together with *EDNRB* and *PTGDS*, followed by activated progenitors and interneurons (fig. S11, D to F). Thus, developmental trajectories that are increased in TSC patient organoids are present in the human fetal brain.

Because phenotypes in TSC organoids arose at later stages of organoid development, we hypothesized that the expanded CGE progenitors might correspond to specific progenitors in the fetal brain (Fig. 3E, red circle).

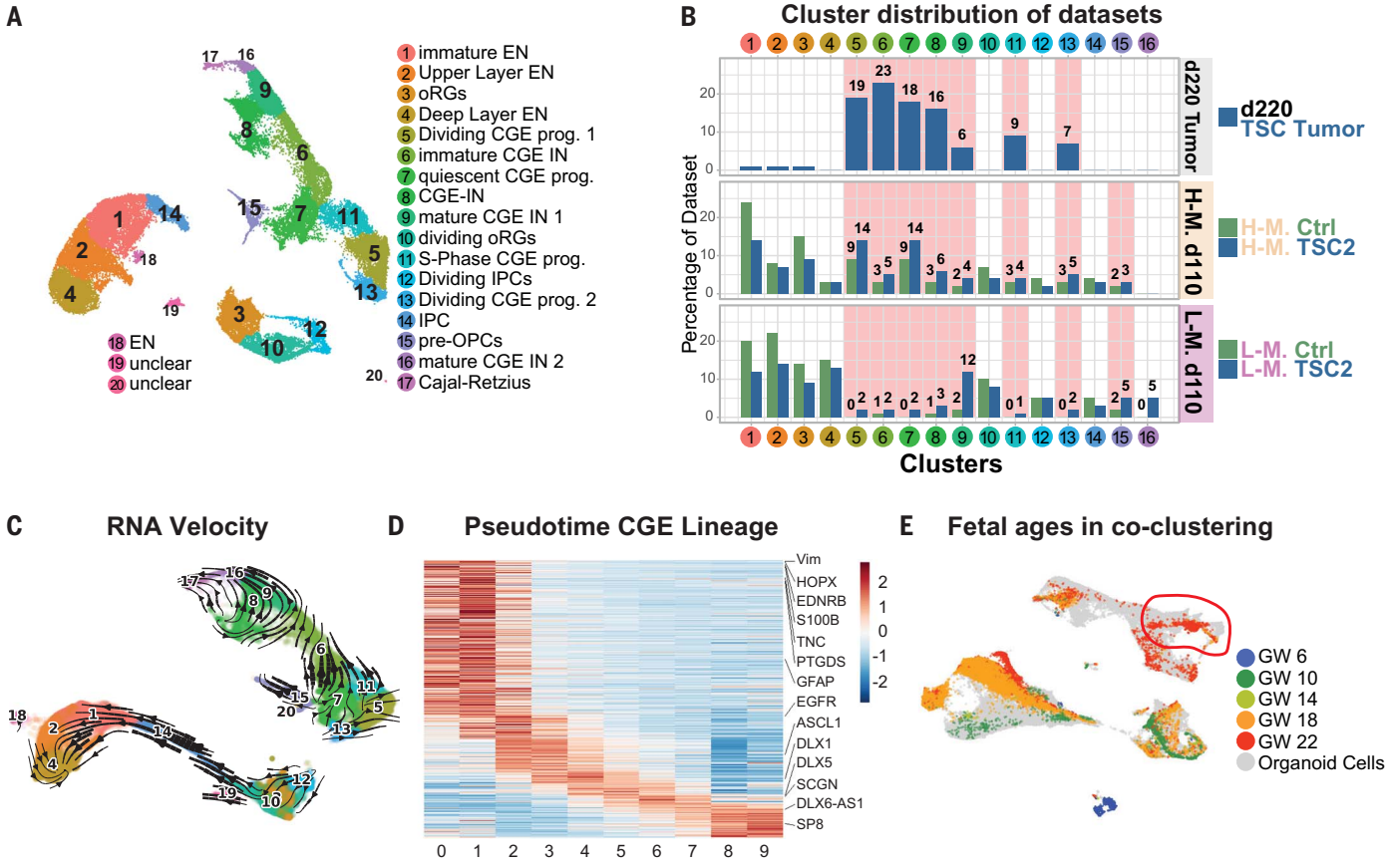

Fig. 3. Late CGE progenitors give rise to TSC phenotypes. (**A**) UMAP projection of 220-day-old TSC tumor organoids with 110-day-old control and *TSC2*$^{+/-}$-derived organoids in H- and L-medium. All cell types of the dorsal lineage were present, with radial glia (RG; clusters 3 and 10), intermediate progenitors (IPCs; clusters 12 and 14), and excitatory neurons (EN; clusters 1, 2, 4, and 18). A separate lineage of CGE-derived cells was identified with quiescent CGE progenitors (cluster 7), dividing CGE progenitor cells (clusters 5, 11, and 13), and CGE interneurons (IN; clusters 6, 8, 9, 16, and 17). Pre-OPC-like cells (cluster 15) cluster close to quiescent CGE progenitors. (**B**) Contribution of different datasets to clusters shown in (A). TSC tumors 220 days old only contributed to CGE progenitors and their progeny (clusters 5, 6, 7, 8, 9, 11, and 13). These clusters were also increased in 110-day-old *TSC2*$^{+/-}$-derived organoids. H-medium enriched for progenitors. L-medium organoids had more mature CGE-INs (clusters 9 and 16). (**C**) RNA velocity projected in two dimensions. The cluster annotation corresponds to (A). From the increased CGE progenitor population, two trajectories emerge: a small trajectory toward pre-OPC cells (cluster 15) and a larger trajectory toward interneurons (clusters 6 and 9). (**D**) Expression of genes along pseudotime in CGE lineage. Genes enriched along pseudotime were calculated, and cells were binned into 10 groups (*x* axis) (fig. S9B). All genes with enriched expression along the trajectory were ordered by using a sliding average. (Top left) Genes enriched in progenitors. (Bottom right) Genes in mature interneurons. Selected genes are highlighted. (**E**) UMAP of integration of organoid and fetal cells color-coded for gestational ages shows that GW22 cells coclustered with (top right) quiescent CGE progenitor cluster.

To test this, we subclustered all progenitors (fig. S11, G and H) and found that 98% of fetal cells coclustering with the expanded CGE progenitors originated from gestational week 22 (GW22) (fig. S11, G, H, and I). We calculated gene modules (*33*) in progenitors (fig. S11J) and compared organoid and fetal progenitors of various stages. Quiescent CGE progenitor cells showed the highest correlation with fetal progenitors from GW22 (+0.74) (fig. S11, K and L). These data suggest that the expanded CGE progenitors emerge around late mid-gestation, a time when cortical tubers and subependymal tumors are first detected in TSC patients (*20*). On the basis of their CGE origin and late emergence, we named the expanded cell type caudal late interneuron progenitor (CLIP) cells.

CLIP cells and their progeny are abundant in tumors

To independently validate our observations in the scRNA-seq experiments, we investigated expression of markers for CGE, medial ganglionic eminence (MGE), and excitatory cells through immunostaining of patient tumor primary tissue and organoids.

We confirmed expression of EGFR in tumors in organoids and in surgically resected SEGAs (Fig. 4A and fig. S12). Consistent with the scRNA-seq results, the CGE interneuron progenitor markers DLX2, COUP-TFII, and SP8 were found in tumors in organoids from three TSC patients (Fig. 4, B and D, and figs. S12 and S13). By contrast, NKX2.1, a marker for MGE progenitors or SATB2, specific for excitatory neurons, was not expressed (Fig. 4D and fig. S14, A and B).

To investigate the origin of TSC tumors in patients, we stained 35GW SENs. Fetal tumors such as their organoid counterparts were enriched in CGE cells, whereas NKX2.1-expressing cells were rare (Fig. 4, E and F, and fig. S14, C and D). By contrast, NKX2.1 has been shown to be expressed in postnatal SEGAs (*34*). We confirmed expression of NKX2.1 (fig. S14E) but found that postnatal tumor cells also expressed CGE markers (fig. S14, E to G). Thus, although fetal SENs consisted mostly of CGE cells, co-expression of NKX2.1 and CGE markers in postnatal SEGAs could suggest aberrant differentiation at later stages or the involvement of other lineages.

To test which lineages can generate tumors in TSC organoids, we used patterning protocols to generate dorsal and ventral forebrain

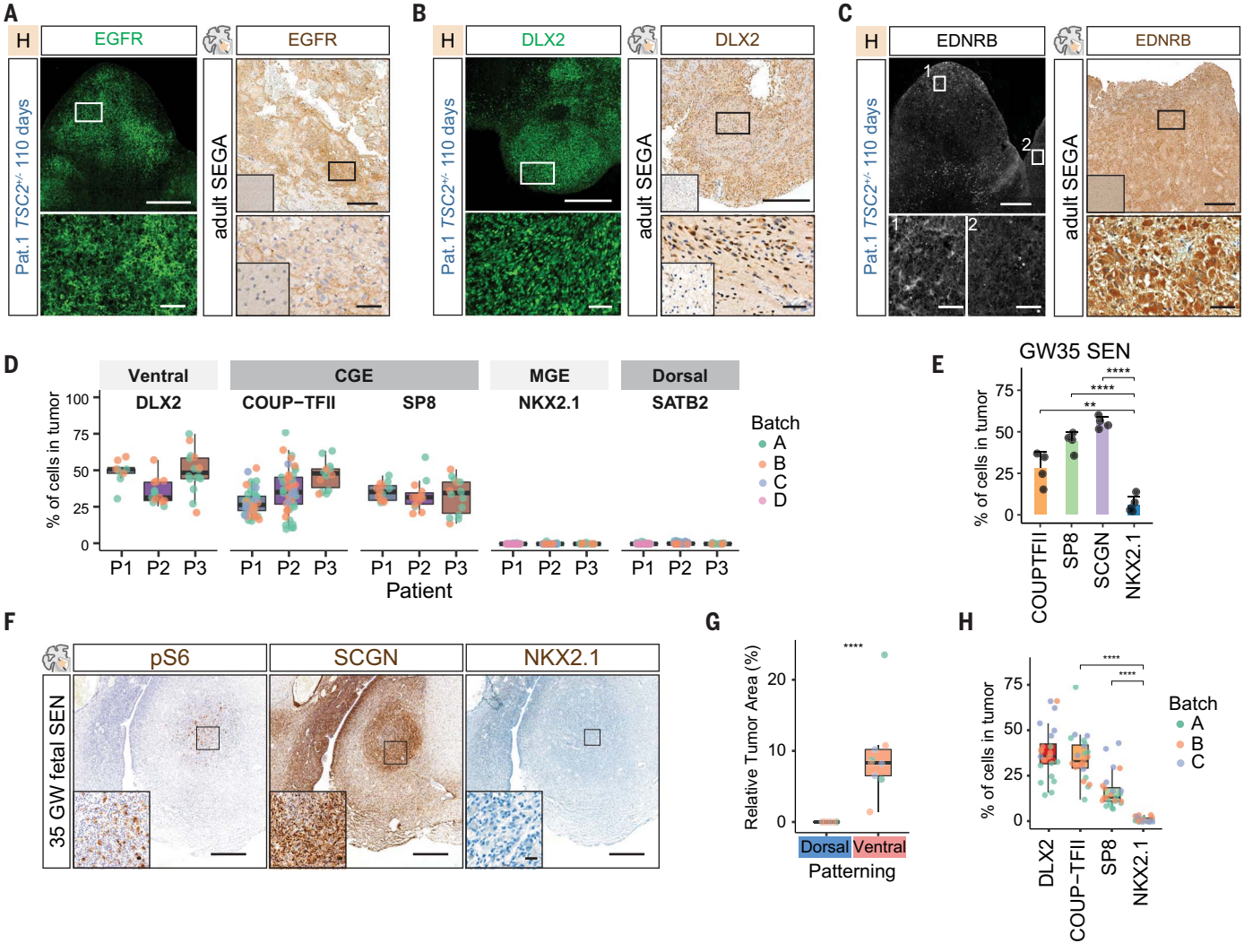

Fig. 4. CGE progenitors initiate TSC tumors. (**A**) Immunostaining for EGFR identified tumors in 110-day-old *TSC2*$^{+/-}$-derived organoids grown in H-medium. EGFR expression was present in adult SEGAs. (Inset) In primary tissue, staining shows healthy control cortex negative for EGFR (costaining with COUP-TFII in organoids is provided in fig. S12C). (**B**) DLX2 was expressed in tumors in 110-day-old *TSC2*$^{+/-}$-derived organoids and resected SEGA tissue. (Inset) In primary tissue, staining shows healthy control cortex negative for DLX2 (fig. S13) (EGFR and SP8 in organoid and patient tumors are provided in fig. S13). (**C**) EDNRB was expressed in tumors in 110-day-old *TSC2*$^{+/-}$-derived organoids. Zoom-ins 1 and 2 are of tumor regions expressing EDNRB and negative region (costaining with PROX1 and pS6 in two patients is provided in fig. S16A). EDNRB expression was found in adult SEGAs. (Inset) In primary tissue, staining shows healthy control cortex negative for EDNRB. (**D**) Quantification of ventral (DLX2), CGE (COUP-TFII and SP8), MGE (NKX2.1), and dorsal markers (SATB2) in tumors of three patients. Tumors of at least two independent batches were quantified, indicated with different colors. Ventral and CGE markers are found in all tumors; MGE and dorsal markers are not found (statistical comparison is provided in fig. S14B). (**E**) Quantification of CGE markers COUP-TFII, SCGN, SP8, and MGE marker NKX2.1 in 35GW fetal SENs (mean and standard deviation) (statistical comparison is provided in fig. S14D). (**F**) Immunostaining on fetal SENs. Fetal tumors characteristically expressed Vimentin (fig. S14C) and pS6 in enlarged cells. Tumor were enriched in SCGN-expressing CGE interneurons. Only a few MGE cells were found. (**G**) Dorsal and ventral patterning of tumors of patient 1. In 120-day-old *TSC2*$^{+/-}$-derived organoids, tumors only appear in ventral patterned organoids that contain interneuron progenitors (Student's *t* test) (an overview of samples is available in fig. S15B). (**H**) Tumors in ventral patterned organoids expressed the ventral marker DLX2 and the CGE markers COUP-TFII and SP8, whereas NKX2.1 is almost absent (ordinary one-way ANOVA with Tukey's multiple comparison test) (statistical comparison is provided in fig. S15H). Scale bars, (A), (B), and (C) overview images, 500 μm; (A), (B), and (C) zoom-ins, 50 μm; (F) overview, 500 μm; (F) inset, 20 μm.

separately (fig. S15A) (*35*, *36*). Dorsal patterning produced excitatory cells, whereas ventral patterned organoids contained both CGE and MGE lineages (fig. S15, C and D). Tumors were only observed in ventral patterned organoids (Fig. 4G and fig. S15B), supporting an origin in the ventral forebrain. All tumors in ventral patterned organoids expressed abundantly the CGE markers COUP-TFII and SP8, whereas only a few cells were positive for NKX2.1 (Fig. 4H and fig. S15, D to H). This further supports the hypothesis that CGE progenitors initiate TSC tumors.

To test whether CGE progenitors in TSC tumors were CLIP cells, we stained for EDNRB and PTGDS. Both patient primary tumor samples and organoid tumors contained cells that expressed these CLIP cell markers together with ventral neural stem cell (NSC) (SOX2 and GAD1) and CGE markers (PROX1 and COUP-TFII) (organoids, EDNRB in Fig. 4C and PTGDS in fig. S16I, with PROX1, COUP-TFII, GAD1, and SOX2 in fig. S16, A, F, and I; surgically removed SEGA, EDNRB in Fig. 4C, with GAD1 in fig. S16,

E and G). These data suggest that CLIP cells are the neural progenitors found in TSC tumors.

Besides CLIP cells, TSC tumors also contained interneurons (Fig. 2, A and B) (*24*). Expression of the CGE interneuron marker SCGN (secretagogin) (fig. S17, A and B) in fetal SENs (Fig. 4F and fig. S17D) and in tumors in organoids (fig. S17C) supported a CGE origin for these interneurons. The lineage relationship between CLIP cells and CGE interneurons was further confirmed with EdU labeling (fig. S17, E and F). After 24 hours, EdU-labeled cells coexpressed either EGFR and SCGN or both, confirming that CLIP cells produce SCGN-positive interneurons (fig. S17, E and F).

Our data indicating that CLIP cells that originate from the CGE generate TSC tumors could provide an explanation for why SEN/SEGAs are typically found in the caudothalamic groove, the region where the CGE is located during fetal development.

CLIP cells initiate cortical tuber development

To determine whether CLIP cells also give rise to GCs that make up cortical tubers, we stained tuber-like structures in L-organoids and tubers in patient-derived brain tissue. GCs in organoids and in fetal cortical tubers expressed markers of ventral NSCs [GAD1) (Fig. 5, A to C, and fig. S19A) and EGFR (figs. S18A and S19D)]. Expression of CLIP cell markers [EDNRB (Fig. 5, D and F) and PTGDS (fig. S18D)] together with CGE markers [PROX1 and COUP-TFII (fig. S18, B to D)] in GCs in organoids underlined their CLIP cell origin. Similarly, expression of EDNRB (Fig. 5E and fig. S19, A and B) and PTGDS with CGE-markers (PROX1 and COUP-TFII) (fig. S19C) further suggested that CLIP cells are also the cell of origin for GCs in TSC patients.

Dysmorphic neurons in cortical tubers have been shown to express excitatory and inhibitory neuron markers (*4*). In addition, early TSC lesions are populated by a high density of migrating neurons of unknown origin (*4*). To determine whether CGE interneurons produced by CLIP cells contribute to cortical tubers, we evaluated expression of CGE (SCGN and COUP-TFII), MGE [Parvalbumin (PV)], and excitatory neuron markers (SATB2) in organoids and patients. We found that at early stages, most dysmorphic neurons in organoids were CGE interneurons (Fig. 5H and fig. S20, A to E). At later stages, the contribution of excitatory neurons increased, whereas only few MGE interneurons are found (Fig. 5, G and H, and fig. S20, F and G).

To test whether CGE interneurons are involved in early tuber lesions in patients, we tested expression of SCGN and PV in a 25GW TSC case. At this stage, tuber pathogenesis initiates with white matter lesions (WMLs). Similar to the organoid model, we found that WMLs were highly enriched in CGE interneurons, whereas no MGE cells were detected (Fig. 5, I and J, and fig. S21, A to D). This suggests that CGE interneurons are the migrating neurons previously described in TSC lesions.

Because excitatory dysmorphic neurons increased over time in organoids, we evaluated the contribution of different lineages during the development of TSC tubers. Around 35GW, CGE interneurons were still increased (Fig. 5, K and L). At the same time, the first dysmorphic neurons (DNs) appeared, with CGE-DNs being more abundant in WMLs. (Fig. 5M and fig. S21E). With progression of tuber lesions at postnatal stages, however, numbers of both excitatory and MGE neurons increased (fig. S22, A to E).

MGE and CGE markers identify distinct populations during normal brain development. In TSC patient organoids, we detected a subpopulation of dysmorphic interneurons expressing the MGE marker PV together with the CGE marker SCGN (fig. S20, G and H). To test whether this misdifferentiated population is present in cortical tubers, we tested expression of PV with the CGE markers SCGN and SP8. In a matched control case, no cells coexpressing these markers were found, whereas in a cortical tuber, several triple-positive cells were detected (fig. S22F). Taken together, our data suggest that CGE lineages initiate cortical lesion development in TSC. Excitatory and MGE dysmorphic neurons appear over time and are frequent in postnatal lesions. Furthermore, our data show that a comprehensive analysis of different markers is necessary to study the contribution of different lineages to cortical tubers because misdifferentiated cells can be observed.

EGFR inhibition reduces tumor burden

mTOR inhibition has been clinically used to treat SEN/SEGAs in TSC patients. However, known side effects and limitations, such as tumor regrowth after drug discontinuation, necessitate exploring alternative therapeutic strategies (*37*–*39*). Both CLIP cells and proliferating cells in TSC tumors express EGFR. To assess the role of the EGFR pathway in tumor growth, we performed a drug testing assay in *TSC2*$^{+/-}$ H-organoids at 110 days, when tumors were already apparent. We used the EGFR receptor tyrosine kinase inhibitor (RTKI) Afatinib and Everolimus, an mTOR Complex 1 inhibitor. Organoids were treated for 30 days with Everolimus, Afatinib, or dimethyl sulfoxide (DMSO) (fig. S23A). Tumor reduction was determined by measuring areas coexpressing pS6 and EGFR. Everolimus treatment almost completely abolished tumors in 140-day-old organoids (Fig. 6, A and B, and fig. S23B). After Afatinib treatment, both tumor load and mean tumor size were significantly reduced when compared with those of untreated organoids (Fig. 6, A and B, and fig. S23, B to D). Thus, targeting the EGFR pathway could be an alternative strategy for the treatment of TSC brain lesions.

We have shown that the neurodevelopmental disorder TSC is initiated by a caudal late interneuron progenitor, the CLIP cells (fig. S24). Early lesions consisted almost exclusively of CLIP cell lineages, whereas other cell types appeared during disease progression. Although our scRNA-seq analysis is descriptive and we only analyzed organoids from one patient, our extensive validation in organoids from three TSC patients plus tissues from more than 10 additional TSC cases demonstrates that the TSC organoid model recapitulated fetal disease dynamics. However, the organoid model was limited in modeling postnatal processes, possibly because of the absence of environmental factors that are present in vivo.

The cell of origin for many human brain tumors remains elusive; however, the idea that cancer stems from the reactivation of a remnant of developmental tissue was proposed more than a century ago (*40*, *41*). Studies in mice have revealed sensitivity of adult neural stem cells to cancer-initiating mutations, resulting in the formation of glioblastoma, a high-grade brain tumor. Transcriptional similarities between CLIP cells and mouse adult neural stem cells suggest that CLIP cells could be involved more generally in brain cancers. Our data suggest that a sensitivity to increased mTOR signaling makes CLIP cells vulnerable to mutations in *TSC2*. We hypothesize that a similar mechanism could explain other malformations of cortical development caused by mTOR dysregulation,such as FCD type II.

Extensive migration of interneurons into the cortex continues in humans even after birth (*42*). Because these late migrating neurons also arise from the CGE and share markers with CLIP cells, we speculate that CLIP cells give rise to late migrating interneurons in the healthy human brain. This is consistent with previous results showing that CGE-derived interneurons contribute to the human brain in much higher percentages (*43*, *44*) and with the observation that late-migrating SCGN interneurons from the CGE are found in humans but not in mice (*45*). The protracted brain development seen in large, gyrated cortices was accompanied by the generation or expansion of cell types. These are not or less present in small lissencephalic brains such as the mouse brain, necessitating human disease models. Our data suggest that CLIP cells are among the cell types specific for or amplified in the human brain, which would make TSC a disease specific to large, gyrated brains.

Materials and methods summary

Detailed information on all materials and methods performed are provided in the supplementary materials.

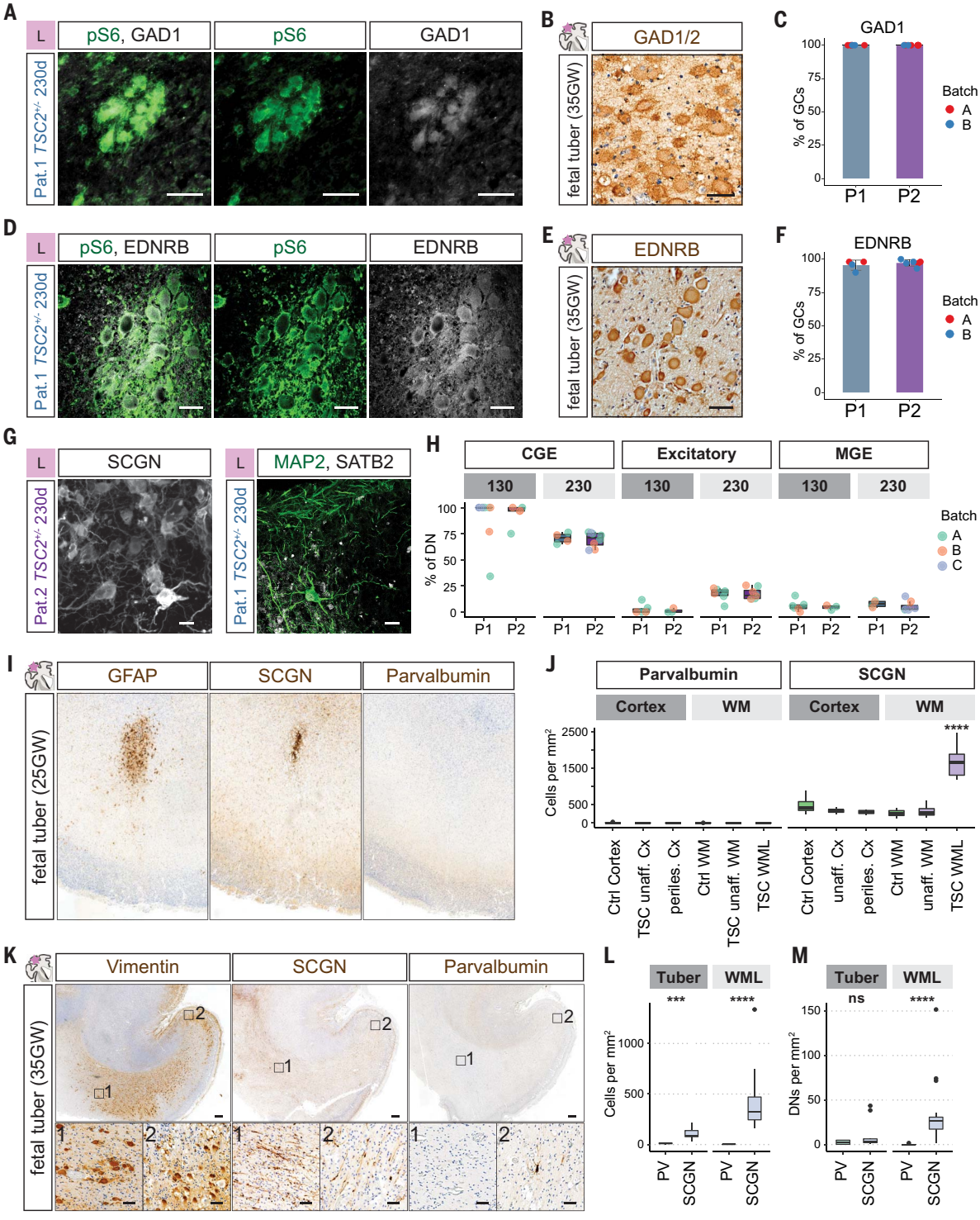

Fig. 5. CLIP cells initiate cortical tuber pathogenesis. (**A** and **B**) GCs in (A) organoids and (B) fetal tubers expressed the interneuron lineage marker GAD1. (**C**) Quantification of coexpression of GAD1 and pS6 in GCs in organoids (patient 1, $N = 2$ independent batches $n = 6$ organoids mean = 100%; patient 2: $N = 2$ independent batches $n = 8$ organoids mean = 100%). (**D** and **E**) EDNRB was expressed in GCs in organoids and in fetal tubers. (**F**) Quantification of coexpression of EDNRB and pS6 in GCs in organoids (patient 1, $N = 2$ independent batches $n = 4$ organoids mean = 95.5%; patient 2: $N = 2$ independent batches $n = 6$ organoids mean = 97.2%). (**G**) Dysmorphic neurons at 230 days expressed the CGE marker SCGN. Individual dysmorphic neurons expressed the excitatory marker SATB2 (stainings at different time points are avilable in fig. S20, C to G). (**H**) Quantification of expression of CGE (SCGN and COUP-TFII), excitatory (SATB2), and MGE markers (PV) in dysmorphic neurons (DNs) at early and late stages in organoids of two patients. CGE DNs were enriched at 130 days and decreased over time. Excitatory DNs increased over time. Statistical analysis is provided in fig. S20, I and J. (**I**) GFAP identified early dysplastic regions at 25GW located in the white matter below the cortex. There was a focal enrichment of SCGN-expressing CGE interneurons, whereas PV expressing MGE interneurons were rare (fig. S21, A and B). (**J**) Quantification of MGE marker PV and CGE marker SCGN in ~25GW fetal brain. Unaffected cortical areas, unaffected white matter, as well as white matter lesions

(WMLs) and adjacent cortex (perilesional cortex) quantified for density of cells expressing PV or SCGN (fig. S21, A and B). WMLs were significantly enriched in CGE interneurons compared with all other regions (one-way ANOVA) (statistical analysis is provided in fig. S12, C and D). (**K**) At 35GW, Vimentin staining identified streams of cells in WMLs and affected cortex. SCGN-expressing cells were abundant in the WMLs and cortex, whereas PV-expressing cells were mainly found in cortical regions. (**L** and **M**) Quantification of MGE marker PV and CGE marker SCGN in 35GW TSC case. Density of all cells is shown in (L), with increase of SCGN cells in tuber and WML areas. In (M), the density of DNs expressing PV and SCGN in tuber and WML areas is shown. SCGN DNs were significantly enriched in WMLs, whereas tubers contained similar density of PV and SCGN cells (all neurons, Tuber $P = 0.0002$, WML $P \leq 0.0001$; DNs, Tuber $P = 0.248$, WML $P \leq 0.0001$; pairwise Wilcoxon test) (an overview of samples is available in fig. S21E). Scale bars, (A), (B), (D), (E), and (K) inset, 50 μm; (G) 20 μm; (I) and (K) overview, 500 μm.

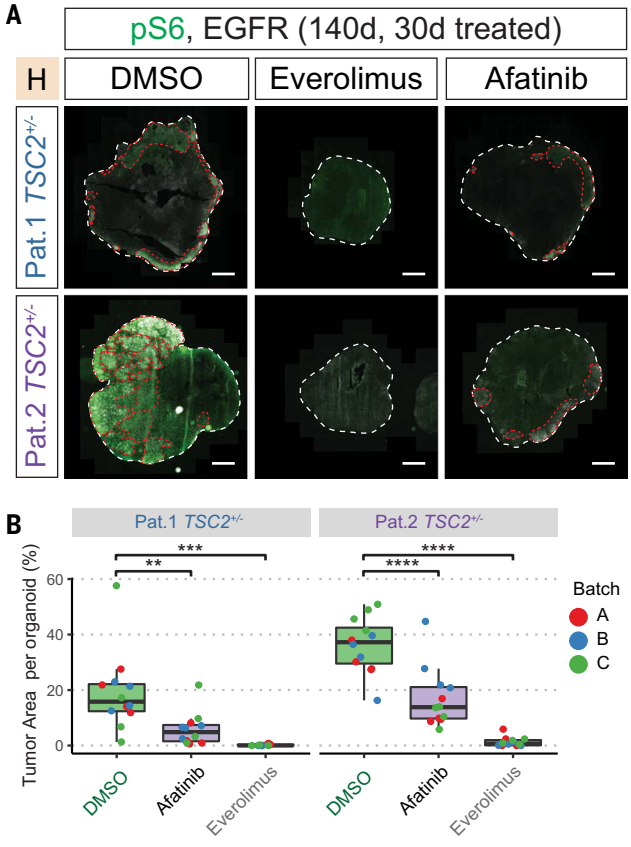

Fig. 6. EGFR inhibition reduces tumor burden. (**A**) Thirty days of treatment started at 110 days after EB formation (fig. S23A). Immunostaining for pS6 and EGFR identified tumors (red lines) in the control group (DMSO) in both patients. Tumors were reduced through Afatinib and Everolimus treatment. (**B**) Quantification of tumor area per organoid. All sections of each organoid stained on one slide were used for quantification. Tumors were identified as regions of overlapping pS6 and EGFR staining. Although tumors were detected in DMSO-control for both patients, Afatinib or Everolimus treatment both reduce tumor burden (two-way ANOVA for treatment condition controlling for batches, Tukey's multiple comparison test) (fig. S23B). Scale bars, (A) 1 mm.

IPS cell generation and culture

Patients were selected from the TSC data registry of the Medical University of Vienna (MUV). Blood was collected from patients, and peripheral blood mononuclear cells (PBMCs) were isolated. Reprogramming was perfomed by using Sendai Vectors. iPSCs cells were cultured by using the Cellartis DEF-CS 500 culture system (Takara). Isogenic control cell lines were directly isolated (mosaic patient 1) or generated by using scarless CRISPR repair (patient 2).

Organoid generation

Organoids were generated by using either a high-nutrient (H-organoids) or low-nutrient (L-organoids) medium to favor proliferation or neuronal maturation, respectively. In addition, organoids were patterned toward dorsal or ventral brain regions as described (*35*, *36*).

Single-cell transcriptomics and analysis

Organoids were dissociated. Library preparation was performed with the Chromium Single Cell 3′ Library and Gel Bead Kit v.3 (10x Genomics, PN-1000075). Libraries were sequenced on a NextSeq 550 (Illumina) or on a NovaSeq SP lane (Illumina). Quality control and preprocessing were performed by use of Seurat R package v.3. Visualization and pseudotime analysis were performed by use of monocle3.

Immunohistochemistry

Immunohistochemistry on frozen organoid samples was performed as described with slight modifications (*18*, *35*). Human brain tissue samples were collected in strict observance of the local legal and institutional ethical regulations. Tissue was processed for cryosections or paraffin sections. Antigen retrieval was performed followed by immunohistochemistry as described in table S6.

REFERENCES AND NOTES

1. R. I. Kuzniecky, MRI in cerebral developmental malformations and epilepsy. *Magn. Reson. Imaging* **13**, 1137–1145 (1995). doi: 10.1016/0730-725X(95)02024-N; pmid: 8750328
2. E. A. Thiele, Managing and understanding epilepsy in tuberous sclerosis complex. *Epilepsia* **51** (Suppl 1), 90–91 (2010). doi: 10.1111/j.1528-1167.2009.02458.x; pmid: 20331728
3. V. Ruppe *et al.*, Developmental brain abnormalities in tuberous sclerosis complex: A comparative tissue analysis of cortical tubers and perituberal cortex. *Epilepsia* **55**, 539–550 (2014). doi: 10.1111/epi.12545; pmid: 24512506
4. A. B. Gelot, A. Represa, Progression of fetal brain lesions in tuberous sclerosis complex. *Front. Neurosci.* **14**, 899 (2020). doi: 10.3389/fnins.2020.00899; pmid: 32973442
5. E. P. Henske, S. Jóźwiak, J. C. Kingswood, J. R. Sampson, E. A. Thiele, Tuberous sclerosis complex. *Nat. Rev. Dis. Primers* **2**, 16035 (2016). doi: 10.1038/nrdp.2016.35; pmid: 27226234
6. K. R. Martin *et al.*, The genomic landscape of tuberous sclerosis complex. *Nat. Commun.* **8**, 15816 (2017). doi: 10.1038/ncomms15816; pmid: 28643795
7. P. B. Crino, Evolving neurobiology of tuberous sclerosis complex. *Acta Neuropathol.* **125**, 317–332 (2013). doi: 10.1007/s00401-013-1085-x; pmid: 23386324
8. D. M. Feliciano, T. Su, J. Lopez, J. C. Platel, A. Bordey, Single-cell Tsc1 knockout during corticogenesis generates tuber-like lesions and reduces seizure threshold in mice. *J. Clin. Invest.* **121**, 1596–1607 (2011). doi: 10.1172/JCI44909; pmid: 21403402
9. D. M. Feliciano, J. L. Quon, T. Su, M. M. Taylor, A. Bordey, Postnatal neurogenesis generates heterotopias, olfactory micronodules and cortical infiltration following single-cell Tsc1 deletion. *Hum. Mol. Genet.* **21**, 799–810 (2012). doi: 10.1093/hmg/ddr511; pmid: 22068588
10. S. W. Way *et al.*, Loss of Tsc2 in radial glia models the brain pathology of tuberous sclerosis complex in the mouse. *Hum. Mol. Genet.* **18**, 1252–1265 (2009). doi: 10.1093/hmg/ddp025; pmid: 19150975
11. R. P. Carson, D. L. Van Nielen, P. A. Winzenburger, K. C. Ess, Neuronal and glia abnormalities in Tsc1-deficient forebrain and partial rescue by rapamycin. *Neurobiol. Dis.* **45**, 369–380 (2012). doi: 10.1016/j.nbd.2011.08.024; pmid: 21907282
12. J. Goto *et al.*, Regulable neural progenitor-specific Tsc1 loss yields giant cells with organellar dysfunction in a model of tuberous sclerosis complex. *Proc. Natl. Acad. Sci. U.S.A.* **108**, E1070–E1079 (2011). doi: 10.1073/pnas.1106454108; pmid: 22025691
13. J. D. Blair, D. Hockemeyer, H. S. Bateup, Genetically engineered human cortical spheroid models of tuberous sclerosis. *Nat. Med.* **24**, 1568–1578 (2018). doi: 10.1038/s41591-018-0139-y; pmid: 30127391
14. W. Qin *et al.*, Analysis of TSC cortical tubers by deep sequencing of TSC1, TSC2 and KRAS demonstrates that small second-hit mutations in these genes are rare events. *Brain Pathol.* **20**, 1096–1105 (2010). doi: 10.1111/j.1750-3639.2010.00416.x; pmid: 20633017
15. E. P. Henske *et al.*, Allelic loss is frequent in tuberous sclerosis kidney lesions but rare in brain lesions. *Am. J. Hum. Genet.* **59**, 400–406 (1996). pmid: 8755927
16. J. A. Chan *et al.*, Pathogenesis of tuberous sclerosis subependymal giant cell astrocytomas: Biallelic inactivation of TSC1 or TSC2 leads to mTOR activation. *J. Neuropathol. Exp. Neurol.* **63**, 1236–1242 (2004). doi: 10.1093/jnen/63.12.1236; pmid: 15624760

17. A. G. Knudson Jr., Mutation and cancer: Statistical study of retinoblastoma. *Proc. Natl. Acad. Sci. U.S.A.* **68**, 820–823 (1971). doi: 10.1073/pnas.68.4.820; pmid: 5279523
18. M. A. Lancaster *et al*., Cerebral organoids model human brain development and microcephaly. *Nature* **501**, 373–379 (2013). doi: 10.1038/nature12517; pmid: 23995685
19. C. Bardy *et al*., Neuronal medium that supports basic synaptic functions and activity of human neurons in vitro. *Proc. Natl. Acad. Sci. U.S.A.* **112**, E2725–E2734 (2015). doi: 10.1073/pnas.1504393112; pmid: 25870293
20. S. H. Park *et al*., Tuberous sclerosis in a 20-week gestation fetus: Immunohistochemical study. *Acta Neuropathol.* **94**, 180–186 (1997). doi: 10.1007/s004010050691; pmid: 9255394
21. M. Mizuguchi, S. Takashima, Neuropathology of tuberous sclerosis. *Brain Dev.* **23**, 508–515 (2001). doi: 10.1016/S0387-7604(01)00304-7; pmid: 11701246
22. A. M. Buccoliero *et al*., Subependymal giant cell astrocytoma: A lesion with activated mTOR pathway and constant expression of glutamine synthetase. *Clin. Neuropathol.* **35**, 295–301 (2016). doi: 10.5414/NP300936; pmid: 27390104
23. A. M. Buccoliero *et al*., Subependymal giant cell astrocytoma (SEGA): Is it an astrocytoma? Morphological, immunohistochemical and ultrastructural study. *Neuropathology* **29**, 25–30 (2009). doi: 10.1111/j.1440-1789.2008.00934.x; pmid: 18564101
24. J. A. Cotter, An update on the central nervous system manifestations of tuberous sclerosis complex. *Acta Neuropathol.* **139**, 613–624 (2020). doi: 10.1007/s00401-019-02003-1; pmid: 30976976
25. C. S. McGinnis *et al*., MULTI-seq: Sample multiplexing for single-cell RNA sequencing using lipid-tagged indices. *Nat. Methods* **16**, 619–626 (2019). doi: 10.1038/s41592-019-0433-8; pmid: 31209384
26. H. V. Vinters *et al*., Tuberous sclerosis-related gene expression in normal and dysplastic brain. *Epilepsy Res.* **32**, 12–23 (1998). doi: 10.1016/S0920-1211(98)00036-9; pmid: 9761305
27. M. W. Johnson, J. K. Emelin, S. H. Park, H. V. Vinters, Co-localization of TSC1 and TSC2 gene products in tubers of patients with tuberous sclerosis. *Brain Pathol.* **9**, 45–54 (1999). doi: 10.1111/j.1750-3639.1999.tb00209.x; pmid: 9989450
28. J. Zhou *et al*., Tsc1 mutant neural stem/progenitor cells exhibit migration deficits and give rise to subependymal lesions in the lateral ventricle. *Genes Dev.* **25**, 1595–1600 (2011). doi: 10.1101/gad.16750211; pmid: 21828270
29. J. S. Lim *et al*., Somatic mutations in TSC1 and TSC2 cause focal cortical dysplasia. *Am. J. Hum. Genet.* **100**, 454–472 (2017). doi: 10.1016/j.ajhg.2017.01.030; pmid: 28215400
30. C. Kerfoot *et al*., Localization of tuberous sclerosis 2 mRNA and its protein product tuberin in normal human brain and in cerebral lesions of patients with tuberous sclerosis. *Brain Pathol.* **6**, 367–375 (1996). doi: 10.1111/j.1750-3639.1996.tb00866.x; pmid: 8944308
31. W. Huang *et al*., Origins and proliferative states of human oligodendrocyte precursor cells. *Cell* **182**, 594–608.e11 (2020). doi: 10.1016/j.cell.2020.06.027; pmid: 32679030
32. A. Bhaduri *et al*., Cell stress in cortical organoids impairs molecular subtype specification. *Nature* **578**, 142–148 (2020). doi: 10.1038/s41586-020-1962-0; pmid: 31996853
33. C. Trapnell *et al*., The dynamics and regulators of cell fate decisions are revealed by pseudotemporal ordering of single cells. *Nat. Biotechnol.* **32**, 381–386 (2014). doi: 10.1038/nbt.2859; pmid: 24658644
34. J. F. Hang *et al*., Thyroid transcription factor-1 distinguishes subependymal giant cell astrocytoma from its mimics and supports its cell origin from the progenitor cells in the medial ganglionic eminence. *Mod. Pathol.* **30**, 318–328 (2017). doi: 10.1038/modpathol.2016.205; pmid: 27910945
35. M. A. Lancaster *et al*., Guided self-organization and cortical plate formation in human brain organoids. *Nat. Biotechnol.* **35**, 659–666 (2017). doi: 10.1038/nbt.3906; pmid: 28562594
36. J. A. Bagley, D. Reumann, S. Bian, J. Lévi-Strauss, J. A. Knoblich, Fused cerebral organoids model interactions between brain regions. *Nat. Methods* **14**, 743–751 (2017). doi: 10.1038/nmeth.4304; pmid: 28504681
37. D. N. Franz *et al*., Everolimus for subependymal giant cell astrocytoma in patients with tuberous sclerosis complex: 2-year open-label extension of the randomised EXIST-1 study. *Lancet Oncol.* **15**, 1513–1520 (2014). doi: 10.1016/S1470-2045(14)70489-9; pmid: 25456370
38. D. A. Krueger *et al*., Long-term treatment of epilepsy with everolimus in tuberous sclerosis. *Neurology* **87**, 2408–2415 (2016). doi: 10.1212/WNL.0000000000003400; pmid: 27815402
39. F. Martins *et al*., A review of oral toxicity associated with mTOR inhibitor therapy in cancer patients. *Oral Oncol.* **49**, 293–298 (2013). doi: 10.1016/j.oraloncology.2012.11.008; pmid: 23312237
40. A. Bhaduri *et al*., Outer radial glia-like cancer stem cells contribute to heterogeneity of glioblastoma. *Cell Stem Cell* **26**, 48–63.e6 (2020). doi: 10.1016/j.stem.2019.11.015; pmid: 31901251
41. S. Sell, Stem cell origin of cancer and differentiation therapy. *Crit. Rev. Oncol. Hematol.* **51**, 1–28 (2004). doi: 10.1016/j.critrevonc.2004.04.007; pmid: 15207251
42. M. F. Paredes *et al*., Extensive migration of young neurons into the infant human frontal lobe. *Science* **354**, eaaf7073 (2016). doi: 10.1126/science.aaf7073; pmid: 27846470
43. D. V. Hansen *et al*., Non-epithelial stem cells and cortical interneuron production in the human ganglionic eminences. *Nat. Neurosci.* **16**, 1576–1587 (2013). doi: 10.1038/nn.3541; pmid: 24097039
44. R. D. Hodge *et al*., Conserved cell types with divergent features in human versus mouse cortex. *Nature* **573**, 61–68 (2019). doi: 10.1038/s41586-019-1506-7; pmid: 31435019
45. C. S. Raju *et al*., Secretagogin is expressed by developing neocortical GABAergic neurons in humans but not mice and increases neurite arbor size and complexity. *Cereb. Cortex* **28**, 1946–1958 (2018). doi: 10.1093/cercor/bhx101; pmid: 28449024
46. O. Eichmüller, OliverEichmueller/TSC_Science2021: Reference scripts. Zenodo (2021); doi: 10.5281/zenodo.5741170

ACKNOWLEDGMENTS

We thank C. da Cunha E Silva Martins Costa, P. Möseneder, H. Eleanor Gustafson, and S. Wolfinger for help with experiments and analyses; the IMBA Stem Cell Core Facility and C. Allison Agu for generation of IPS Cell Lines; B. Gebarski and A. Vogt for library preparation and sequencing performed at the VBCF NGS Unit (www.viennabiocenter.org/facilities/next-generation-sequencing); the Genome Engineering Unit of VBCF ProTech facility (http://www.viennabiocenter.org/facilities/protein-technologies) for assistance with isogenic control line preparation; K. Stejskal and E. Roitinger for mass spectrometry performed at the IMBA/IMP mass spectrometry facility; the IMBA/IMP Biooptics facility; A. Mancebo Gimenez and M. Zeba of the VBCF HistoPathology facility for immunohistochemistry; A. Meixner for coordinating ethical approvals; R. Diehm; G. Kasprian for providing MRIs; the KIN Biobank of the Medical University of Vienna (MUV); K. Auguste and the UCSF Brain Tumor SPORE Biorepository (NIH/NCI 5P50CA097257) for their coordination for surgical tissue collection; V. Elorriaga Benavides for work on primary material; and O. Wüseke for establishing contact with the MUV. We thank G. Riddihough/Life Science Editors for help with editing the initial version of the manuscript. We especially thank all patients and their families for participating in this study or donating tissue. **Funding:** A.V. was supported by an EMBO Fellowship (ALTF-1112-2019). Work in J.A.K.'s laboratory is supported by the Austrian Federal Ministry of Education, Science and Research, the Austrian Academy of Sciences, the City of Vienna, and the SFB F78 Stem Cell (F 7803-B). This project has received funding from the European Research Council (ERC) under the European Union's Horizon 2020 research and innovation (695642). **Author contributions:** O.L.E, N.S.C., M.F., and J.A.K. designed the study and analysis. Experiments were performed by O.L.E., I.M., N.S.C., T.S., V.-E.G., A.M.P., and J.C. Data analysis was performed by O.L.E., N.S.C., J.A.H., A.V., M.N., and M.F.P. The study was supervised by N.S.C. and J.A.K. The manuscript was prepared by O.L.E, N.S.C., and J.A.K., with input from all authors. **Competing interests:** J.A.K. is on the supervisory and scientific advisory board of a:head bio AG (https://aheadbio.com) and is an inventor on several patents relating to cerebral organoids. **Data and materials availability:** WGS and scRNA-seq data are available through controlled access at the European genome-phenome Archive (EGA). Study number, EGAS00001004586. Datasets: single cell RNA-seq, EGAD00001006332; whole genome sequencing, EGAD00001006333. All code used in this study is available on GitHub (https://github.com/OliverEichmueller/TSC_Science2021), Zenodo (*46*), and upon request. TSC patient IPS cell lines will be made available upon request after obtaining ethical approval from the Ethics Committee of MUV under a materials transfer agreement with the Institute of Molecular Biotechnology of the Austrian Academy of Sciences. This study was approved by the local ethics committee of MUV.

SUPPLEMENTARY MATERIALS

science.org/doi/10.1126/science.abf5546
Materials and Methods
Figs. S1 to S24
References (*47*–*59*)
Tables S1 to S7
MDAR Reproducibility Checklist

View/request a protocol for this paper from *Bio-protocol*.

3 November 2020; resubmitted 14 June 2021
Accepted 6 December 2021
10.1126/science.abf5546